Geophysical Research Letters

RESEARCH LETTER
10.1029/2022GL098186

Precipitation in Northeast Mexico Primarily Controlled by the Relative Warming of Atlantic SSTs

Kevin T. Wright[1], Kathleen R. Johnson[1], Tripti Bhattacharya[2], Gabriela Serrato Marks[3], David McGee[3], Dillon Elsbury[1,4,5], Yannick Peings[1], Jean-Louis Lacaille-Muzquiz[6], Gianna Lum[1], Laura Beramendi-Orosco[7], and Gudrun Magnusdottir[1]

[1]Deptment of Earth System Science, University of California, Irvine, Irvine, CA, USA, [2]Department of Earth Sciences, Syracuse University, Syracuse, NY, USA, [3]Department of Earth, Atmospheric and Planetary Sciences Massachusetts Institute of Technology, Cambridge, MA, USA, [4]Cooperative Institute for Research in Environmental Sciences, Boulder, CO, USA, [5]NOAA Chemical Sciences Laboratory, Boulder, CO, USA, [6]Independent Researcher, Ciudad Mante, Mexico, [7]Instituto de Geología, Universidad Nacional Autónoma de México, Ciudad Universitaria, Ciudad de México, México

Key Points:

- We present the first speleothem record spanning the last millennium from NE Mexico using multiple geochemical proxies
- In contrast to tree ring reconstructions, we suggest regional precipitation is primarily controlled by Atlantic sea-surface temperatures (SSTs)
- We utilize results from a forced-SST climate model to further support our interpretation

Supporting Information:

Supporting Information may be found in the online version of this article.

Correspondence to:

K. T. Wright,
ktwright@uci.edu

Citation:

Wright, K. T., Johnson, K. R., Bhattacharya, T., Marks, G. S., McGee, D., Elsbury, D., et al. (2022). Precipitation in Northeast Mexico primarily controlled by the relative warming of Atlantic SSTs. *Geophysical Research Letters*, *49*, e2022GL098186. https://doi.org/10.1029/2022GL098186

Received 7 FEB 2022
Accepted 6 MAY 2022

Abstract Reconstructing hydroclimate over the Common Era is essential for understanding the dominant mechanisms of precipitation change and improving climate model projections, which currently suggest Northeast Mexico will become drier in the future. Tree-ring reconstructions have suggested regional rainfall is primarily controlled by Pacific sea-surface temperatures (SSTs). However, tree ring records tend to reflect winter-spring rainfall, and thus may not accurately record total annual precipitation. Using the first multiproxy speleothem record spanning the last millennium, combined with results from an atmospheric general circulation model, we demonstrate mean annual rainfall in Northeast Mexico is highly sensitive to Atlantic SST variability. Our findings suggest future precipitation in Northeast Mexico is more dependent upon the warming of Tropical Atlantic SSTs relative to the Tropical Pacific.

Plain Language Summary We use geochemical markers of past rainfall in a rock from a cave (speleothem) to show that warming in Atlantic sea-surface temperatures (SSTs) increases the amount of precipitation in Northeast Mexico. These finding are surprising, since previous rainfall reconstructions using tree rings have suggested a warmer Atlantic decreases precipitation in the region. We used a climate model to show that warming in the Atlantic increases precipitation during the summer but decreases precipitation during the winter. Although winter precipitation only accounts for 8% of annual rainfall in this region, tree rings are more reflective of the winter precipitation response. This is the first speleothem record from NE Mexico over this time-period and suggests that projections of future rainfall should emphasize relative changes in Atlantic SST variability because it has a major impact on annual precipitation.

1. Introduction

Recent droughts in Mexico have led to significant economic crises, national food shortages and mass migrations, greatly impacting over 127 million people (Hunter et al., 2013). Unfortunately, climate models suggest anthropogenic carbon emissions are likely to increase the frequency and intensity of droughts in the future. However, climate models poorly resolve detailed patterns of present and historic rainfall throughout most of Mexico and Central America, exhibiting particularly poor skill in modeling natural internal climate variability (Bhattacharya & Coats, 2020; Deser et al., 2020; Hidalgo et al., 2013). Additionally, a growing body of tropical rainfall records imply future droughts may not be as dire as models project, as the region may receive increased precipitation in response to a warmer climate (He & Soden, 2017; Sachs et al., 2009); though, it remains unclear if increased precipitation will extend to Northern Mexico. Paleoclimate constraints on the response of regional precipitation to internal climate variability and external forcing is thus of utmost importance for evaluating climate models and mitigating the impacts of future rainfall change, yet few records exist in Northern Mexico.

Tree ring records based on classical dendroclimatology (tree ring width) suggest interannual to multidecadal hydroclimate variability in Mexico is dominated by changes in Eastern Equatorial Pacific (EEP) sea surface temperatures (SSTs), primarily associated with the El Niño Southern Oscillation (ENSO) and to a lesser magnitude, the lower frequency Pacific Decadal Oscillation. Warm EEP SSTs are thought to drive a dipole precipitation pattern, with wet conditions in Northern Mexico and dry conditions in Southern Mexico. While drying in Southern Mexico in response to warmer EEP SSTs has been confirmed with paleoclimate records and modeling

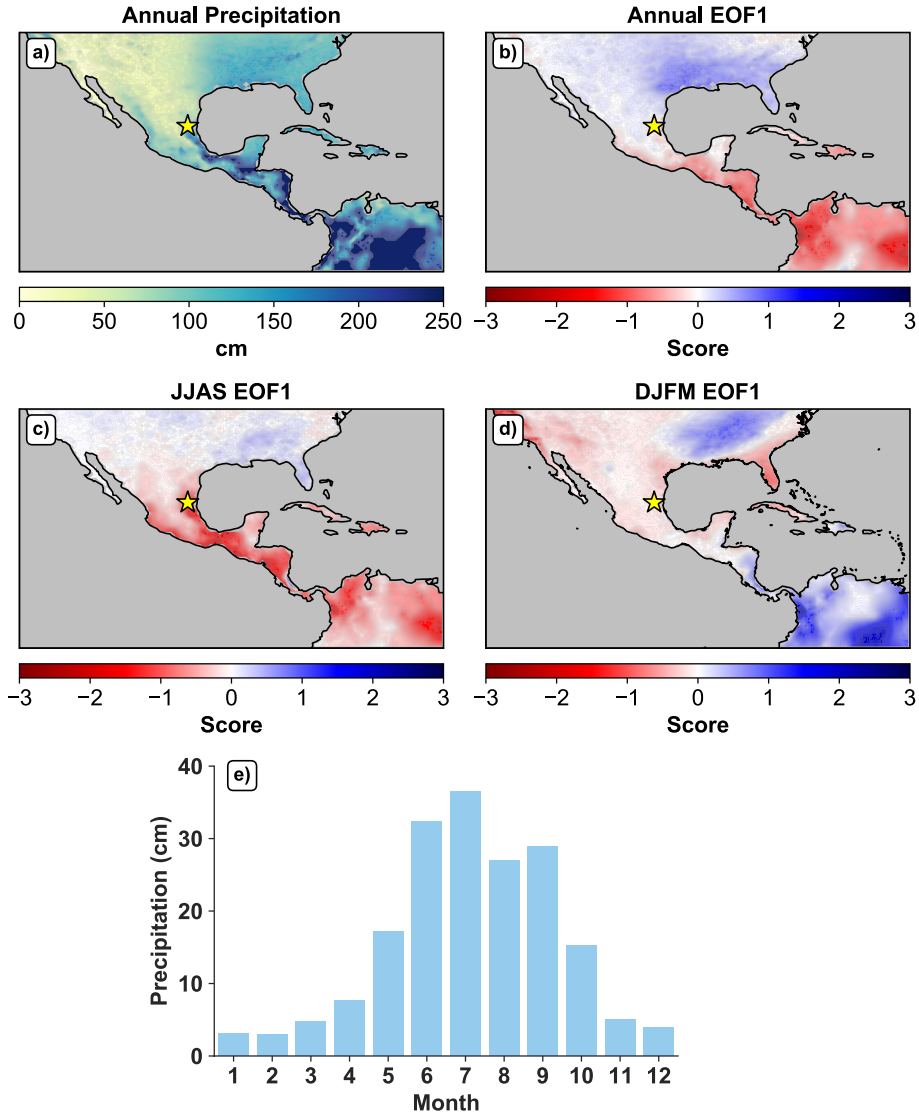

Figure 1. Precipitation data from GPCC (Schneider et al., 2011), showing (a) Mean annual precipitation over Mexico, Central America, and the Circum-Caribbean region, (b) EOF1 of annual precipitation, (c) EOF1 of summer (JJAS) precipitation, and (d) EOF1 of winter (DJFM) precipitation. Panel (e) shows mean monthly precipitation near Cueva Bonita (http://clicom-mex.cicese.mx/).

studies (Bhattacharya & Coats, 2020; Kennett et al., 2012; Lachniet et al., 2012; Medina-Elizalde et al., 2010), increased precipitation in Northeast Mexico remains poorly constrained, with weaker than expected or inconsistent correlations in instrumental records, classical tree ring width data, and tree ring isotopic data (Gutiérrez-García et al., 2020; Stahle et al., 2016; Villanueva-Diaz et al., 2007). Discrepancies between records could potentially be driven by the well-known bias of tree ring width to preferentially record winter-spring precipitation, which may not be reflective of total annual precipitation (Villanueva-Diaz et al., 2007; Wise & Dannenberg, 2019). This may be particularly important in a region such as NE Mexico, which only receives 8% of annual rainfall during boreal winter (DJFM, Figure 1e). Surprisingly, the role of SSTs in the Tropical North Atlantic, the dominant source of moisture for Mexico, remains enigmatic and could obscure the effect of Pacific SSTs. For instance, a positive phase of the Atlantic Multidecadal Variability (AMV) has been invoked to explain broad drying in Northeast Mexico (Stahle et al., 2016). However, instrumental data (Curtis, 2008) and tree ring records from nearby Texas (Gray et al., 2004), as well as records of runoff on interannual to orbital scales from Northeast and Central Mexico (Roy et al., 2016, 2020; Wogau et al., 2019), suggest warmer Atlantic SSTs may drive the opposite response, increasing precipitation. While speleothem records from Northern Mexico covering

the more recent past (Common Era) can provide a robust record of past hydroclimate variability to help clarify the role of Atlantic versus Pacific SSTs on regional precipitation, none have been published in this critical region.

To address this gap, we have developed the first continuous inter-annually resolved stalagmite record (CB4) of past hydroclimate spanning the last millennium utilizing four geochemical proxies: stable oxygen isotopes ($\delta^{18}O$), carbon isotopes ($\delta^{13}C$), trace elements (Mg/Ca), and dead carbon proportion (DCP, based on ^{14}C). Moreover, novel forced-SST climate modeling experiments are employed to confirm precipitation change measured in speleothem CB4. The CB4 sample was retrieved from Cueva Bonita (23°N, 99°W; 1,071 m above sea level) located in the northern-most tropical cloud forest on the windward side of the Sierra Madre Oriental in the Northeast state of Tamaulipas (Figures 1 and S1 in Supporting Information S1). The climate of NE Mexico is characterized by a warm wet summer and a cool dry winter (JJAS; Figure 1e). The stalagmite age model is constrained by 19 U-Th dates and fluorescent annual lamina counting (Figure S2 in Supporting Information S1), and extends from 833 CE to 2017 CE, when the sample was collected (Supporting Information S1). Previous research has often interpreted $\delta^{18}O$ as a proxy for weighted mean annual precipitation amount (Baker et al., 2020), which we also demonstrate is the predominant influence on $\delta^{18}O$ at Cueva Bonita (Figure S3 in Supporting Information S1). However, a growing number of studies have shown that $\delta^{13}C$, Mg/Ca, and DCP are also potentially reliable proxies for local water balance (Griffiths et al., 2020), improving our interpretation of hydroclimate when combined with speleothem $\delta^{18}O$ (see Text S1 in Supporting Information S1).

2. Data and Methods

2.1. Chronology

The CB4 stalagmite was cut, polished and sampled for 15 U-Th dates along its vertical growth axis using a Dremel hand drill with a diamond dental bur. The CB4 sample has uranium concentrations ranging from 37 to 160 ng/g (Table S1 in Supporting Information S1). Calcite powder samples weighing 250–300 mg were prepared at Massachusetts Institute of Technology following methods similar to Edwards et al. (1987). Powders were dissolved in nitric acid and spiked with a ^{229}Th – ^{233}U–^{236}U tracer, followed by isolation of U and Th by iron co-precipitation and elution in columns with AG1-X8 resin. The isolated U and Th fractions were analyzed using a Nu Plasma II-ES multi-collector inductively coupled plasma mass spectrometer (MC-ICP-MS) equipped with an Aridus 2 desolvating nebulizer, following methods described in Burns et al. (2016). The corrected ages were calculated using an initial $^{230}Th/^{232}Th$ value of 9.8 ± 4.9 ppm to correct for initial ^{230}Th. The 9.8 ppm initial Th correction value was determined by testing dates corrected with different initial ^{230}Th corrections for stratigraphic order following methods laid out by Hellstrom (2006) and matching the ages with the radiocarbon bomb peak depth. The uncertainty of 4.9 ppm was scaled proportionally to the normal ±50% correction (4.4 ± 2.2 ppm). U-Th ages range from 78 ± 96 to 2119 ± 162 years before present, however, this study focused on the top 100 mm of the sample with an oldest date of 1189 ± 154 (where present is 1950 CE). All 15 dates fall in stratigraphic order within 2σ uncertainty (Table S1 in Supporting Information S1), but two were identified to be outliers based on low probability of fit for age models (Figure S2 in Supporting Information S1). U-Th ages were combined with fluorescent layer counting to decrease uncertainty. The 95% confidence interval for the age-depth model was constructed using 2000 Monte-Carlo simulations through the age-depth modeling software COPRA (Breitenbach et al., 2012).

2.2. Stable Isotope and Trace Element Analysis

CB4 was micro-sampled for both stable isotope and trace element analyses using a Sherline micromill at 250 µm increments to a depth of 1 mm, producing 400 samples. The powder for CB4 was collected, weighed out to 40–80 µg and analyzed on a Kiel IV Carbonate Preparation Device coupled to a Thermo Scientific Delta V-IRMS at the UC Irvine Center for Isotope Tracers in Earth Sciences (CITIES) following methods described by McCabe-Glynn et al. (2013) to determine $\delta^{18}O$ and $\delta^{13}C$. Every 32 samples of unknown composition were analyzed with 14 standards which included a mix of NBS-18, IAEA-CO-1, and an in-house standard. The analytical precision for $\delta^{18}O$ and $\delta^{13}C$ is 0.08‰ and 0.05‰, respectively.

For trace element analysis, 20–60 µg calcite powder samples were dissolved in 500 µL of a double distilled 2% nitric acid solution. The samples were analyzed using a Nu Instruments Attom High Resolution Inductively

Coupled Plasma Mass Spectrometer (HR-ICP-MS) at the CITIES laboratory. Mg/Ca ratios were calculated from the intensity ratios using a bracketing technique with five standards of known concentration and an internal standard (Ge) added to all samples to correct for instrumental drift. Trace element analysis of CB4 serves to complement the interpretation of speleothem $\delta^{18}O$ and $\delta^{13}C$; therefore, a lower-resolution (multi-decadal to centennial) analysis was conducted over the complete record by analyzing every other sample (200 total; Table S3 in Supporting Information S1). For plotting/aesthetic purposes, CB2 Mg/Ca, $\delta^{18}O$ and $\delta^{13}C$ were smoothed using a moving average. The pandas function DataFrame.rolling().mean() was utilized to smooth the data for plotting only, with the size of the moving window set to 4 years. The full data set reported in Supporting Information S1 is unsmoothed.

2.3. Controls of Modern $\delta^{18}O_{precip}$

Speleothem $\delta^{18}O$ ($\delta^{18}O_{speleo}$) is primarily controlled by precipitation $\delta^{18}O$ ($\delta^{18}O_{precip}$) and cave temperature when calcite is deposited under close to isotopic equilibrium conditions (Fairchild et al., 2006; Hendy, 1971; Lachniet, 2009). In low-to-mid latitude regions, cave temperature has a minimal impact and variations in $\delta^{18}O_{precip}$ dominate the signal. Paleoclimate interpretation of $\delta^{18}O_{speleo}$ may be complicated, though, by the multiple factors that influence $\delta^{18}O_{precip.}$ In the tropics, $\delta^{18}O_{precip}$ has historically reflected the "amount effect" (Dansgaard, 1964), with more precipitation leading to more negative $\delta^{18}O$ values. However, more recent analyses suggest rainfall $\delta^{18}O$ is also dependent on processes taking place on more regional scales. For instance, temperature (Lachniet & Patterson, 2009), shifting moisture sources (Aggarwal et al., 2004; Vuille & Werner, 2005), local moisture recycling (Sánchez-Murillo et al., 2016), orographic effects (Sánchez-Murillo et al., 2013), rainout history (Lachniet et al., 2007), microphysical cloud processes (Bony et al., 2008; Konecky et al., 2019; Risi et al., 2008), storm type (Frappier et al., 2007), and relative proportions of stratiform and convective precipitation (Aggarwal et al., 2016) have all been suggested to influence the oxygen isotope composition of rainfall. A comparison between $\delta^{18}O_{precip}$ to local rainfall amount above Cueva Bonita (Figure S3 in Supporting Information S1), however, suggests precipitation $\delta^{18}O_{precip}$ is inversely correlated to precipitation amount ($r = -0.88$, $p < 0.05$), consistent with the "amount effect" (Dansgaard, 1964). These results are reproduced by IsoGSM data from 1979 to 2015, which demonstrate $\delta^{18}O_{precip}$ in NE Mexico is closely related to local and regional precipitation amount (Wright et al., 2021; Yoshimura et al., 2008). Lastly, speleothem and precipitation records from Southern Mexico have also demonstrated a strong amount effect (Bernal et al., 2011; Lachniet et al., 2012, 2017; Lases-Hernández et al., 2020; Medina-Elizalde et al., 2010; Pérez Quezadas et al., 2015). While other processes may exert secondary influence on $\delta^{18}O_{precip}$, we interpret $\delta^{18}O_{precip}$ (and consequently $\delta^{18}O_{speleo}$) to dominantly be reflective of precipitation amount. Nevertheless, to minimize the uncertainty of our paleoclimate interpretation, we have applied a multi-proxy approach, using the additional $\delta^{13}C$, Mg/Ca, and DCP proxies which are strongly tied to local water balance (See Supporting Information S1).

2.4. Radiocarbon Laboratory Methods

Calcite samples were analyzed for ^{14}C at the University of California, Irvine within the Keck Carbon Cycle Accelerator Mass Spectrometry laboratory. Calcite powders were leached with 10% HCl acid, to remove any secondary carbonates, and hydrolyzed with 85% phosphoric acid. Using a modified hydrogen-reduction method (Beverly et al., 2010), samples were then graphitized via Fe catalyzed hydrogen reduction. During data processing calcite powder from a radiocarbon free speleothem was used for blank subtraction. ^{14}C results were used in combination with the U-Th and lamina counting-based age model to calculate DCP, using IntCal13 data for the atmospheric ^{14}C activity at the time of speleothem formation (Genty et al., 1999; Reimer et al., 2013). For methods used to convert radiocarbon results to DCP see Supporting Information S1.

Variable DCP measurements, such as those measured in sample CB4, have been shown in previous speleothem studies to be indicative of hydrological changes above the cave (Bajo et al., 2017; Griffiths et al., 2012, 2020; Noronha et al., 2015). The exact mechanism of varying DCP is site specific but changes are commonly driven by the response of soil organic matter and open- versus closed-system bedrock dissolution (Fohlmeister et al., 2011; Griffiths et al., 2012). A fully open dissolution system occurs when conditions are dry and cave drip water dissolved inorganic carbon in the epikarst is in complete isotopic equilibrium with modern ^{14}C values. In this scenario, the DCP would be equal to 0% (Hendy, 1971). Alternatively, closed system dissolution occurs when conditions are wet, and water in the voids and fractures of the epikarst are in isotopic exchange with

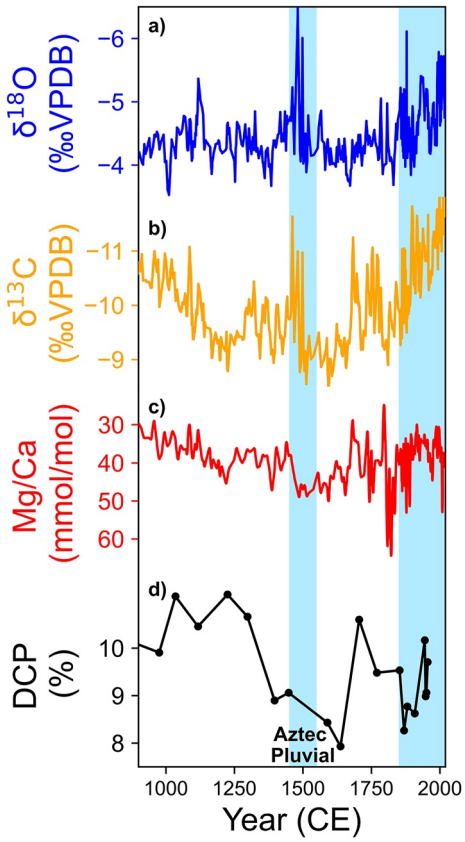

Figure 2. Results of CB4 geochemical proxies. Speleothem (a) $\delta^{18}O$, (b) $\delta^{13}C$, (c) Mg/Ca ratios and (d) dead carbon proportion (DCP) over the last millennium. Speleothem $\delta^{18}O$ and $\delta^{13}C$ have an average resolution of 3 years, Mg/Ca ratios have an average resolution of 6 years, and DCP has an average resolution of 83 years. Results of CB4 proxies show a similar response on multi-decadal to centennial timescales. Compared to $\delta^{18}O$, proxies show a moderate to strong correlation on multidecadal timescales ($\delta^{13}C$, $r = 0.56$, $p < 0.05$; Mg/Ca, $r = 0.29$, $p < 0.05$). Shading in blue represents wet periods during the Aztec Pluvial at ~1450, and during the industrial period (~1800–2017).

both the atmosphere and the bedrock. Therefore, the upper limit of DCP in a completely closed system would be 50% (Bajo et al., 2017; Hendy, 1971; Noronha et al., 2015). Of course, most DCP values in natural cave systems are somewhere between these extremes, with caves demonstrating an average DCP of 15 ± 5% (Genty et al., 1999). The average CB4 DCP values fall within the low side of this range and are 9.5 ± 0.9%. Given the multitude of controls of $\delta^{18}O$, $\delta^{13}C$ and Mg/Ca (Johnson, 2021), DCP provides an additional hydroclimate proxy.

2.5. Forced SST Model Simulations

As a complement to the proxy records, we use general circulation model experiments to isolate the atmospheric response to each possible combination of sea surface temperature anomalies associated with AMV and Interdecadal Pacific Variability (IPV). We use the specified chemistry version of the Whole Atmosphere Community Climate Model with Community Atmosphere Model version 4 physics (Marsh et al., 2013; Smith et al., 2015). The model domain extends from the surface up to 145 km over 66 vertical levels with a horizontal resolution of 1.9 by 2.5° latitude and longitude.

Given that the AMV and IPV can exist in positive (warm tropics), negative (cool tropics), or neutral states, there are nine combinations of SST variability that are used to force the model. The neutral AMV/neutral IPV experiment serves as the control. It is a 200-year continuous integration of the model that is forced with a fixed repeating annual cycle of present-day SST/sea ice concentration variability (1979–2008 average annual cycle from the Hadley Centre Sea Ice and Sea Surface Temperature data set - HadISST (Rayner et al., 2003).

To obtain the anomalous SSTs corresponding to the AMV and IPV, external drivers of climate variability (solar and volcanic) and anthropogenic forcing (greenhouse gasses and aerosols) must be removed from the long-term SST record. The external forcing to the SSTs is obtained by applying signal-to-noise maximizing EOF analysis (Ting et al., 2009) to a global mean SST record derived from a CMIP5 multimodel ensemble of historical (1870–2005) and Representative Concentration Pathway 8.5 (2006–2013) data. The difference between the spatial pattern of "observed" Extended and Reconstructed SST version 4 (ERSSTv4, Huang et al., 2015) data and the spatial pattern of SSTs corresponding to the aforementioned forced component yields the internal SST variability from which the AMV and IPV patterns are obtained following subsequent filtering for low-frequency (decadal) variability and construction of AMV/IPV indices (see technical note 1 from Boer et al., 2016; Elsbury et al., 2019). The AMV/IPV simulations are identical to the control except that the SST patterns (Figure S4 in Supporting Information S1) corresponding to each combination of AMV and IPV are superimposed on top of the control simulation SSTs and then integrated for 200 years. The precipitation, sea level pressure (SLP) and low-level wind anomalies shown in Figure 4 were produced by differencing the atmospheric fields in these perturbation simulations from that of the control. The AMV index utilized in Figure 3 was created using a detrended, 121-month smoothed, area weighted average of Kaplan SST data set over the N. Atlantic from 0 to 70°N (Enfield et al., 2001).

3. Results and Discussion

3.1. Warmer Atlantic SSTs Drive Extended Wet Periods in NE Mexico

The most striking centennial-scale feature of this record is the extremely low speleothem $\delta^{18}O$ values of −6.5‰ at ~1490 CE (Figure 2), which is also supported by very low $\delta^{13}C$ values (−11‰) and Mg/Ca ratios (38 mmol/mol) near the same time. Increased precipitation during the 15th century has been suggested as a dominant driver

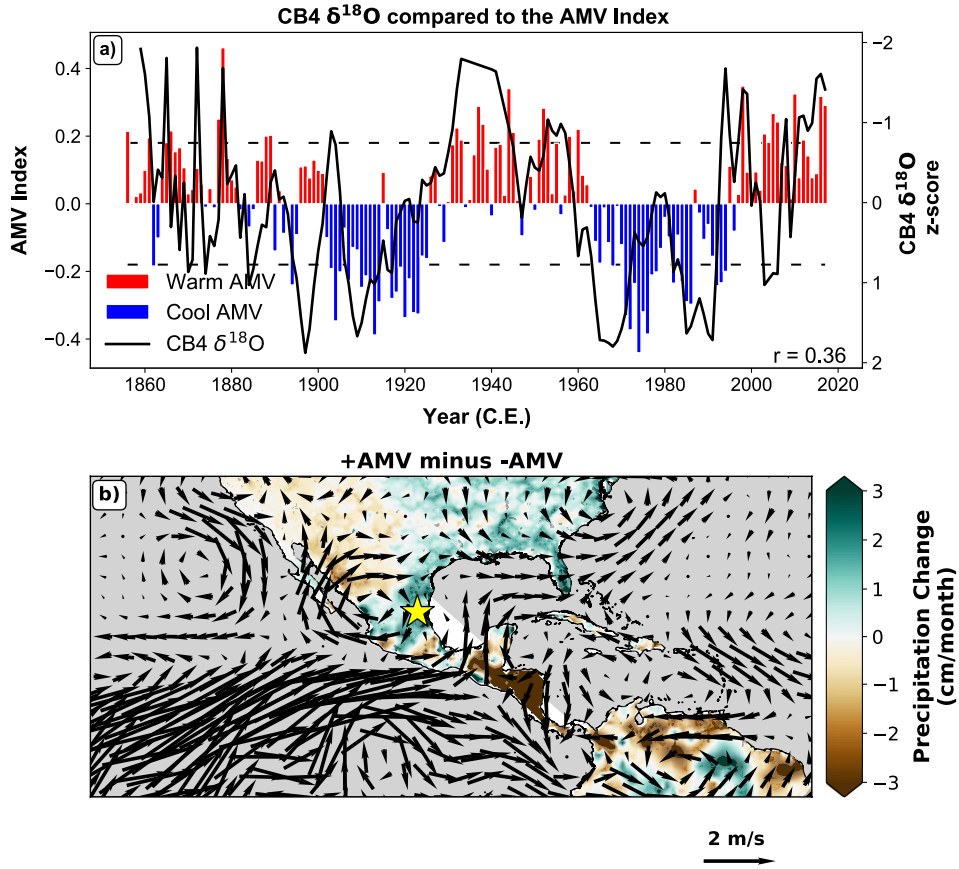

Figure 3. Comparison of Atlantic Multidecadal Variability (AMV) to CB4 $\delta^{18}O$, precipitation and low-level winds. (a) The AMV index is provided by NOAA and Kaplan sea surface temperatures (SSTs) (Enfield et al., 2001). Both the CB4 and Atlantic SSTs are detrended to account for the impact of anthropogenic warming. The $\delta^{18}O$ appears to capture both extended periods of positive phases (1920–1960, 2000–2020+) and extended negative phases (1900–1920, 1960–2000) of the AMV index over the last 150 years. (b) Comparison of AMV phases (positive [2000–2010] minus negative [1980–1990]) on mean low-level winds and precipitation anomalies. A positive phase leads to increased precipitation in NE Mexico but drying in NW and Southern Mexico.

of population expansion at major archeological sites, including Tenochtitlan in the Basin of Mexico, and has thus been referred to as the Aztec Pluvial (Sanders et al., 1979). Stahle et al. (2016) provided evidence that the Aztec Pluvial could be a major wet period over the Common Era but lacked older tree ring records to confirm the magnitude and spatial extent of increased precipitation. Our record confirms through multiple geochemical proxies that the Aztec Pluvial represented the wettest conditions in Northeast Mexico over the last millennium. Speleothem $\delta^{18}O$ from Juxtlahuaca cave in SW Mexico and Ti concentration in lake sediments from Central Mexico also show increased precipitation during this interval (Lachniet et al., 2017; Wogau et al., 2019), suggesting the Aztec Pluvial impacted at least Northeast, Central and Southwest Mexico, if not the entire country. While a strengthening of the North American Monsoon has been invoked to explain increased precipitation in Southwest and Central Mexico (Lachniet et al., 2017), NE Mexico is outside the monsoon's dominant core region, suggesting a strengthened monsoon is not likely the primary mechanism for increased precipitation at this time. A comparison of Cueva Bonita $\delta^{18}O$ to Eastern and Tropical North Atlantic SSTs instead suggests the 15th century pluvial period was likely forced by anomalously warm Atlantic SSTs (Figures S5 and S6 in Supporting Information S1). Warmer SSTs are known to increase precipitation in NE Mexico by increasing boundary layer moisture convergence, as well as favoring the development of hurricanes (Wang & Lee, 2007). These results are consistent with reconstructions from the Last Millennium Reanalysis Project (Anderson et al., 2019) which show: (a) Tropical Atlantic SSTs are similar to modern values, (b) Reduced sea-level pressures over the Gulf of Mexico, likely favoring deep convective storm activity, and (c) Increased precipitation in NE Mexico (Figure S7 in Supporting Information S1).

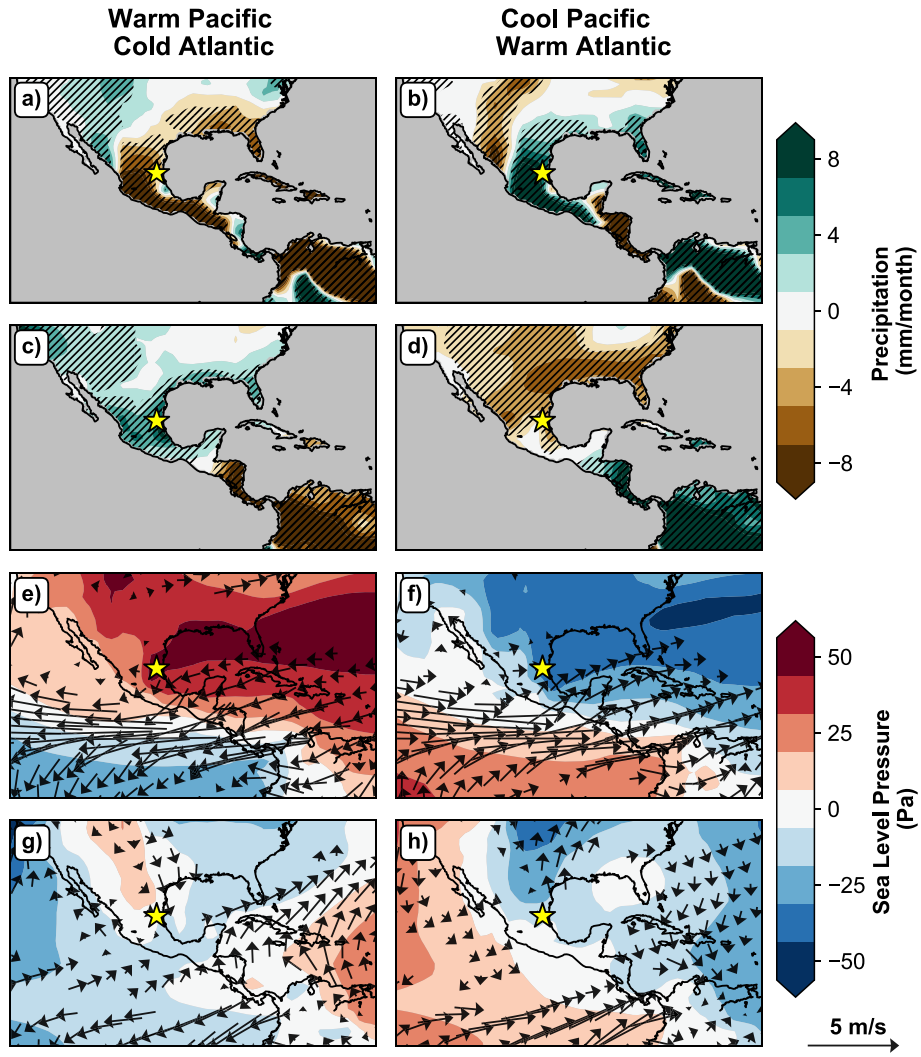

Figure 4. Precipitation, sea level pressure (SLP), and low-level winds in response to forced sea surface temperatures (SSTs). (a–d) Results of net precipitation change in the forced-SST simulations. Statistically significant changes (90% CI) are indicated by hatching. (e–h) Results of anomalous low-level wind patterns and SLP in response to forced SST simulations. Changes in SLPs are indicated by color; only statistically significant SLP and low-level winds are plotted. Summer results are shown in panels (a, b, e, and f) and winter results are show in panels (c, d, g, and h). Cueva Bonita location is indicated by the star.

Notably, the CB4 record also indicates a pattern of decreasing $\delta^{18}O$ values (from −3.5‰ – −6.7‰) beginning near the end of the pre-industrial period, around 1830. This trend is also supported by a shift toward more negative $\delta^{13}C$ values (−8.9‰ – −13‰), decreased Mg/Ca ratios (54–28 mmol/mol), and increased DCP suggesting increased precipitation with anthropogenic warming is robust across multiple geochemical proxies. The decreasing trend of $\delta^{18}O$ and $\delta^{13}C$ appears to be in response to Atlantic warming, as Pacific warming is delayed until the early- to mid-20th century (Figure S6 in Supporting Information S1). Interestingly, this trend toward wetter conditions is not obvious in Mexican tree rings (Stahle et al., 2016), but is evident in historical precipitation records, satellite data and re-analysis data from Central Mexico (Martinez-Lopez et al., 2018), suggesting precipitation increases may occur only in summer and early autumn. Although our record is not sub-annually resolved to verify, we suggest the wetting trend may be driven by more extreme pluvial climate events in the late-summer and early-autumn months. This interpretation is supported by evidence for increased tropical cyclone rainfall rates (Knutson et al., 2019) and increased precipitation from more slowly decaying hurricanes on land over the last century (Li & Chakraborty, 2020). Furthermore, extremely wet hurricanes are projected to increase in frequency, making historic flooding (1 in 2000-year) events such as that caused by Hurricane Harvey much more likely (1

in 100-year) by 2100 CE (Emanuel, 2017). Overall, the CB4 record combined with recent analysis of extreme pluvial events suggests NE Mexico could become wetter under anthropogenic climate change.

3.2. The Influence of Pacific and Atlantic SSTs on Multidecadal Hydroclimate Variability

The strong positive correlation of NE Mexico rainfall to Atlantic SSTs is surprising, considering tree ring records have provided robust evidence of spatially widespread drying in response to positive phases of the AMV (Stahle et al., 2016). However, our record demonstrates a strong positive correlation to Atlantic SSTs not only on centennial timescales but on multidecadal timescales as well. This is evident in a direct comparison of proxies over the last ~800 years (Figures S5 and S6 in Supporting Information S1), wavelet power spectrum analysis demonstrating a periodicity of 66 years for $\delta^{18}O$ and 55 years for $\delta^{13}C$ (Figure S8 in Supporting Information S1), which is close to the previously suggested periodicity of 65 years for the AMV (Schlesinger & Ramankutty, 1994), and a direct comparison of the AMV index to CB4 $\delta^{18}O$ over the last century (Figure 3a). From lake sediment reconstructions of runoff in NE Mexico, Roy et al. (2016) speculated that the AMV likely altered regional hydroclimate during the early Holocene and Late-Pleistocene but the records did not retain the temporal resolution required to verify the impact of the AMV on regional precipitation. Our record provides the first multiproxy evidence of AMV influence on NE Mexico precipitation over the last millennium.

Interestingly, CB4 proxies not only stand in contrast to tree ring interpretations of the role of Atlantic SSTs, but speleothem $\delta^{18}O$, $\delta^{13}C$, and Mg/Ca ratios also record wetter conditions during periods of cool Eastern Pacific SSTs, a response also reflected in additional speleothem records from Southern Mexico and Central America (Lachniet et al., 2004, 2017). The similarity in speleothem records across both Northern and Southern Mexico suggests precipitation may not be out-of-phase in these two regions as previously thought (Bhattacharya & Coats, 2020; Méndez & Magaña, 2010; Stahle et al., 2016). Modern instrumental data also suggests precipitation is mostly in-phase during seasonal (summer) and annual timescales (Figure 1) and only shows a strong dipole precipitation pattern for winter rainfall (Figures 1 and S1 in Supporting Information S1). While changes in winter-spring soil moisture, as typically recorded by tree ring chronologies, are closely linked to changes in early summer soil moisture, they can be poorly correlated with late summer and autumn rainfall (Stahle et al., 2016; St. George et al., 2010). Furthermore, most low-elevation, sub-tropical and tropical tree ring reconstructions from North America are biased toward recording dry extremes while completely missing wet extremes, especially during the summer (Wise & Dannenberg, 2019). Given that summer precipitation in NE Mexico accounts for ~70% of total annual rainfall (Figure 1e), we suggest the discrepancies between the speleothem data presented here and tree ring-based interpretations are driven by the winter-spring moisture bias of tree rings. While analysis of instrumental data supports this notion, with a positive phase of the AMV leading to increased precipitation in NE Mexico (Figure 3b), historical rainfall is complicated as it is also impacted by Pacific variability and complex forcing of Atlantic variability on the Pacific, and vice versa (Bhattacharya & Coats, 2020).

3.3. Forced SST Model Simulations and Mechanisms of Precipitation Change

To test the seasonality and spatial pattern of rainfall in response to SST variability, we utilized a state-of-the-art general circulation model with prescribed patterns of Atlantic and Pacific SST variability. This experimental design allows us to disentangle the influence of the Pacific variability on the Atlantic, and vice-versa. Control runs of this model reliably capture global patterns of observational precipitation and low-level winds (Smith et al., 2015), including Mexico and Central America (Figures S9 and S10 in Supporting Information S1). While our analysis includes a full range of forced-SST conditions (Figures S11–S14 in Supporting Information S1), the natural environment on interannual to decadal timescales is most likely to exhibit an Atlantic-Pacific out-of-phase warming or cooling via changes in the strength of the Walker Circulation (Fosu et al., 2020), and are therefore the focus of this discussion.

During summer, in response to a warm Pacific and cold Atlantic, precipitation decreases across almost all of Mexico and Central America (Figure 4a). Anomalous convection in the Pacific in response to warmer conditions has previously been attributed to drying via an enhanced Walker Circulation, which is also simulated in this study (Figures 4a and S11c in Supporting Information S1). This results in a southward migration of the Atlantic ITCZ and stronger easterly trade winds (Bhattacharya & Coats, 2020; Bhattacharya et al., 2017; Chiang & Sobel, 2002; Giannini et al., 2000, 2001). While the contraction of the ITCZ is known to decrease precipitation in Southern

Mexico and Central America (Asmerom et al., 2020), stronger easterly trade winds are thought to increase precipitation in Northern Mexico via an intensification of easterlies and the Caribbean Low-Level Jet (CLLJ) (Wang & Lee, 2007). Although low-level wind anomalies in model simulations correctly replicate the intensification of the CLLJ (Figure S10 in Supporting Information S1), models demonstrate a stronger CLLJ instead leads to decreased precipitation over much of Mexico (Figures 4b and 4f). This response is also replicated when SST conditions are reversed, which drives a weakening of the CLLJ and increased precipitation (Figured 4b and 4c). On longer orbital to interannual timescales, a stronger CLLJ has been linked to drier conditions in NE Mexico through Atlantic SST cooling and an enhanced wind-evaporation-SST feedback loop (Wright et al., 2021). However, this experiment utilizes prescribed SSTs and we therefore cannot attribute observed precipitation changes to this mechanism. We instead suggest that warmer Atlantic SSTs lead to a reduction in the strength of the CLLJ and, consequently, a reduction in vertical wind shear. Decreased vertical wind shear appears to be further amplified by cooler Pacific SSTs (Figure S14 in Supporting Information S1), which fosters the formation of deep convective storms and increases precipitation throughout most of Mexico (Figure 4b). This mechanism is further supported by observational records and previous modeling results (Wang, 2007; Wang & Lee, 2007), which have linked decreased vertical wind shear to more frequent and larger magnitude hurricanes in the Tropical North Atlantic.

Another notable result of the fixed SST simulations is the contrasting response of precipitation throughout most of Mexico during summer and winter (Figures 4a and 4b vs. 4c and 4d, Figure S13 in Supporting Information S1). The only region that appears to respond consistently in both seasons is Northwest Mexico, which is strongly influenced by the North American Monsoon and is likely to be more sensitive to variability in Pacific SSTs. In response to a warm Pacific/cold Atlantic, winter precipitation throughout much of Mexico slightly increases (Figure 4c). Increased winter precipitation in Northwest and Central Mexico has been attributed to a strengthening of the North Pacific storm-track extending further south and west in response to anomalous waves (Seager & Hoerling, 2014). While this is not likely to drive increased precipitation as far east as NE Mexico (Wright et al., 2021), warmer Pacific SSTs could drive more frequent and intensified cold fronts from the North, increasing light, low-intensity rainfall to the region (Magana et al., 2003). This interpretation is consistent with results presented here, where anomalous northerly low-level winds are produced by forced-SST experiments (Figure 4g).

When SST conditions are reversed during winter (warm Atlantic/cold Pacific), model results suggest there is a reversal in the low-level winds pattern, leading to drier conditions (Figure 4h). This is consistent with the response recorded in tree rings which have suggested drier conditions during a positive phase of the AMV (Méndez & Magaña, 2010; Stahle et al., 2016). Previous work has suggested warmer Atlantic SSTs reduce the interbasin SST and SLP gradient, which weakens the CLLJ leading to decreased moisture transport to Northern Mesoamerica and increased precipitation in Southern Mesoamerica (Bhattacharya & Coats, 2020; Bhattacharya et al., 2017; Mestas-Nuñez et al., 2007; Stahle et al., 2016). Although a decreased and southward diverging CLLJ is reproduced in this study (Figure 4h), producing the north-south dipole precipitation pattern (Figure 4d), we believe the decrease in northern frontal storms is a more important mechanism for reducing precipitation in NE Mexico since a weaker CLLJ tends to increase precipitation during summer months (Figures 4b and 4f). Therefore, winter simulations of rainfall support tree ring interpretations of: (a) an out-of-phase dipole spatial pattern, and (b) a dominant role of Pacific SSTs in controlling regional precipitation. However, winter precipitation (DJFM) only accounts for a small fraction of total annual rainfall, with winter contributing less than 8% of annual rainfall in NE Mexico (Figure 1e). We therefore suggest relative changes in Atlantic SSTs are much more important in controlling total annual precipitation amount in the region.

The new CB4 speleothem record from NE Mexico combined with forced-SST climate model results highlights the precipitation dipole pattern is far more spatially complex in Mexico than previously thought (Figures S15 and S16 in Supporting Information S1). We suggest previous reconstructions of the dipole pattern may have utilized tree rings that are potentially biased toward winter, spring, or early-summer rainfall (Stahle et al., 2016, 2020), minimizing the role of the Atlantic in modulating late-summer and early-autumn precipitation throughout most of the region. While variability in Pacific SSTs can still play an important secondary role in regulating precipitation, we suggest warmer Pacific SSTs predominantly drive decreased precipitation over the region. We instead propose that warmer Atlantic SSTs drive increased precipitation in the region by increasing summer precipitation, which accounts for 70% of total annual rainfall in the region (Figure 1e).

4. Conclusions

Anthropogenic carbon emissions will continue to warm Tropical Atlantic SSTs in the future (Chen et al., 2018). Given the observed trend of increased precipitation in NE Mexico over the industrial period indicated by decreasing CB4 $\delta^{18}O$, this suggests NE Mexico could become wetter in the future, in contrast to current model projections. Importantly, though, forced-SST experiments show that precipitation in Mexico is most sensitive to the warming of the Tropical Atlantic relative to the Tropical Pacific. Unfortunately, models currently exhibit significant discrepancies in determining this interbasin SST gradient, greatly decreasing confidence in regional rainfall projections (Bhattacharya & Coats, 2020). In part, this is further underscored by the fact that models produce different SST responses to external forcing (volcanic vs. orbital) even over the last millennium (Bhattacharya & Coats, 2020). Furthermore, SST biases in the eastern Tropical Pacific and the Tropical Atlantic, driven by poor model representation of topography in Mesoamerica (Baldwin et al., 2021) and oceanic and atmospheric circulation (Imbol Nkwinkwa et al., 2021), further confound the ability to accurately reproduce the SST interbasin gradient. Lastly, the large inter-model spread in precipitation is also partially driven by the paucity of paleoclimate records and uncertainties in the response of rainfall and SSTs to internal variability (Deser et al., 2020). By using a model with prescribed SSTs based on observational data, this study was able to circumnavigate some of these issues and highlight conditions and mechanisms that drive precipitation change in Mexico. However, accurate projections of future rainfall will necessitate improvements in model SST sensitivity to various forcings, more accurate topography, better representation of atmospheric circulation, and a robust understanding of the response of precipitation to internal variability. In addition, improved constraints on precipitation isotope controls, through increased modern sampling and detailed analyses of isotope-enabled climate model simulations of the region, are an important area for future study that could further strengthen paleoclimatic interpretations.

We suggest robust proxy records of past hydroclimate such as CB4 be utilized in future studies to isolate models that best reproduce both the amount and temporal pacing of precipitation variability. Given the demonstrated dependence of precipitation on regional SSTs, we believe these models will also accurately simulate large scale interactions between the Pacific and Atlantic (i.e., the interbasin gradient), which has important implications for predicting hydroclimate in other regions as well. Particularly, annual to sub-annual speleothem records would be ideal to confirm precipitation during the dominantly wet summer season and for the direct evaluation of ENSO, which unfortunately was not possible given the temporal resolution of CB4. Overall, however, CB4 is an important contribution to the paleoclimate record in this critically understudied region. We have provided four independent hydrological proxies of past precipitation change over the last millennium and have validated the proposed mechanisms of precipitation change utilizing forced-SST experiments. We hope this study will serve as the foundation for future work in Northern Mexico.

Conflict of Interest

The authors declare no conflicts of interest relevant to this study.

Data Availability Statement

Speleothem stable isotope, trace element and dead carbon proportion data utilized to reconstruct precipitation from CB4 is available at https://www.ncei.noaa.gov/access/paleo-search/study/36436. Radiocarbon and U-Th results are included in Tables in Supporting Information S1 (Supplementary Material) and available at https://www.ncei.noaa.gov/access/paleo-search/study/36436. Version 1.15 of the COPRA depth-age modeling software utilized to build the age model in this study is available at https://doi.org/10.5194/cp-8-1765-2012. Data for the atmospheric general circulation model experiments is available at https://doi.org/10.5281/zenodo.6388371. GPCC Precipitation data provided by the NOAA/OAR/ESRL PSL, Boulder, Colorado, USA, from their Web site at https://psl.noaa.gov/data/gridded/data.gpcc.html.

Acknowledgments
We thank Cheva Berrones-Benitez for her assistance with rainfall sampling. We thank Jim Kennedy, Esteban Berrones, Corinne Wong, and Chris Wood for their help with fieldwork. We thank Dachun Zhang, Jessica Wang, Chris Wood, and Elizabeth Patterson for assistance with lab work. We thank Crystal Tulley-Cordova for sharing the precipitation collector design. This research was supported by a UC MEXUS-CONACYT Collaborative Grant from the University of California Institute for Mexico and the United States (UC MEXUS CN-16-120), an MIT International Science and Technology Initiatives Mexico Program, and National Science Foundation awards AGS-1804512 and AGS-1806090. K. R. Johnson., D. McGee., K. T. Wright, and L. Beramendi-Orosco designed the study; K. T. Wright, G. S. Marks, K. R. Johnson, and J.-L. Lacaille Muzquiz conducted fieldwork; K. T. Wright, G. S. Marks, G.R.G., and G. Lum conducted laboratory analyses; K. T. Wright and D. Elsbury conducted paleoclimate model simulations; K. T. Wright, D. Elsbury, Y. Peings and G. Magnusdottir analyzed model data; K. T. Wright and K. R. Johnson wrote the manuscript with help from coauthors. All authors contributed to data analysis and interpretation.

References

Aggarwal, P. K., Fröhlich, K., Kulkarni, K. M., & Gourcy, L. L. (2004). Stable isotope evidence for moisture sources in the Asian summer monsoon under present and past climate regimes. *Geophysical Research Letters*, *31*(8), L08203. https://doi.org/10.1029/2004GL019911

Aggarwal, P. K., Romatschke, U., Araguas-Araguas, L., Belachew, D., Longstaffe, F. J., Berg, P., et al. (2016). Proportions of convective and stratiform precipitation revealed in water isotope ratios. *Nature Geoscience*, *9*(8), 624–629. https://doi.org/10.1038/ngeo2739

Anderson, D. M., Tardif, R., Horlick, K., Erb, M. P., Hakim, G. J., Noone, D., et al. (2019). Additions to the last millennium reanalysis multiproxy database. *Data Science Journal*, *18*(1), 1–11. https://doi.org/10.5334/dsj-2019-002

Asmerom, Y., Baldini, J. U. L., Prufer, K. M., Polyak, V. J., Ridley, H. E., Aquino, V. V., et al. (2020). Intertropical convergence zone variability in the Neotropics during the Common Era. *Science Advances*, *6*(7), 3644–3658. https://doi.org/10.1126/sciadv.aax3644

Bajo, P., Borsato, A., Drysdale, R., Hua, Q., Frisia, S., Zanchetta, G., et al. (2017). Stalagmite carbon isotopes and dead carbon proportion (DCP) in a near-closed-system situation: An interplay between sulphuric and carbonic acid dissolution. *Geochimica et Cosmochimica Acta*, *210*, 208–227. https://doi.org/10.1016/j.gca.2017.04.038

Baker, A., Berthelin, R., Cuthbert, M. O., Treble, P. C., Hartmann, A., & KSS Cave Studies Team, T. (2020). Rainfall recharge thresholds in a subtropical climate determined using a regional cave drip water monitoring network. *Journal of Hydrology*, *587*, 125001. https://doi.org/10.1016/j.jhydrol.2020.125001

Baldwin, J. W., Atwood, A. R., Vecchi, G. A., & Battisti, D. S. (2021). Outsize influence of Central American orography on global climate. *AGU Advances*, *2*(2), e2020AV000343. https://doi.org/10.1029/2020av000343

Bernal, J. P., Lachniet, M., McCulloch, M., Mortimer, G., Morales, P., & Cienfuegos, E. (2011). A speleothem record of Holocene climate variability from southwestern Mexico. *Quaternary Research*, *75*(01), 104–113. https://doi.org/10.1016/j.yqres.2010.09.002

Beverly, R. K., Beaumont, W., Tauz, D., Ormsby, K. M., vonReden, K. F., Santos, G. M., & Southon, J. R. (2010). The keck carbon cycle AMS laboratory, University of California, irvine: Status report. *Radiocarbon*, *52*(2), 301–309. https://doi.org/10.1017/S0033822200045343

Bhattacharya, T., Chiang, J. C. H., & Cheng, W. (2017). Ocean-atmosphere dynamics linked to 800–1050 CE drying in mesoamerica. *Quaternary Science Reviews*, *169*, 263–277. https://doi.org/10.1016/j.quascirev.2017.06.005

Bhattacharya, T., & Coats, S. (2020). Atlantic-Pacific gradients drive last millennium hydroclimate variability in mesoamerica. *Geophysical Research Letters*, *47*(13), e2020GL088061. https://doi.org/10.1029/2020GL088061

Boer, G. J., Smith, D. M., Cassou, C., Doblas-Reyes, F., Danabasoglu, G., Kirtman, B., et al. (2016). The decadal climate prediction project (DCPP) contribution to CMIP6. *Geoscientific Model Development*, *9*(10), 3751–3777. https://doi.org/10.5194/gmd-9-3751-2016.,

Bony, S., Risi, C., & Vimeux, F. (2008). Influence of convective processes on the isotopic composition ($\delta^{18}O$ and δD) of precipitation and water vapor in the tropics: 1. Radiative-convective equilibrium and tropical ocean–global atmosphere–coupled ocean-atmosphere response experiment (TOGA-COARE) simulations. *Journal of Geophysical Research*, *113*(D19), 19305. https://doi.org/10.1029/2008JD009942

Breitenbach, S. F. M., Rehfeld, K., Goswami, B., Baldini, J. U. L., Ridley, H. E., Kennett, D. J., et al. (2012). Constructing proxy records from age models (COPRA). *Climate of the Past*, *8*(5), 1765–1779. https://doi.org/10.5194/cp-8-1765-2012

Burns, S. J., Godfrey, L. R., Faina, P., Mcgee, D., Hardt, B., Ranivoharimanana, L., & Randrianasy, J. (2016). *Rapid human-induced landscape transformation in Madagascar at the end of the first millennium of the Common Era*. https://doi.org/10.1016/j.quascirev.2016.01.007

Chen, Y., Langenbrunner, B., & Randerson, J. T. (2018). Future drying in central America and northern south America linked with Atlantic Meridional overturning circulation. *Geophysical Research Letters*, *45*(17), 9226–9235. https://doi.org/10.1029/2018GL077953

Chiang, J. C. H., & Sobel, A. H. (2002). Tropical tropospheric temperature variations caused by ENSO and their influence on the remote tropical climate. *Journal of Climate*, *15*(18), 2616–2631. https://doi.org/10.1175/1520-0442(2002)015<2616:TTTVCB>2.0.CO;2

Curtis, S. (2008). The Atlantic Multidecadal Oscillation and extreme daily precipitation over the US and Mexico during the hurricane season. *Climate Dynamics*, *30*(4), 343–351. https://doi.org/10.1007/s00382-007-0295-0

Dansgaard, W. (1964). Stable isotopes in precipitation. *Tellus*, *16*(4), 436–468. https://doi.org/10.3402/tellusa.v16i4.8993

Deser, C., Lehner, F., Rodgers, K. B., Ault, T., Delworth, T. L., DiNezio, P. N., et al. (2020). Insights from Earth system model initial-condition large ensembles and future prospects. *Nature Climate Change*, *10*(4), 277–286. https://doi.org/10.1038/s41558-020-0731-2

Edwards, R. L., Chen, J. H., & Wasserburg, G. J. (1987). $^{238}U^{234}U^{230}Th^{232}Th$ systematics and the precise measurement of time over the past 500, 000 years. *Earth and Planetary Science Letters*, *81*(2–3), 175–192. https://doi.org/10.1016/0012-821X(87)90154-3

Elsbury, D., Peings, Y., Saint-Martin, D., Douville, H., & Magnusdottir, G. (2019). The atmospheric response to positive IPV, positive AMV, and their combination in boreal winter. *Journal of Climate*, *32*(14), 4193–4213. https://doi.org/10.1175/JCLI-D-18-0422.1

Emanuel, K. (2017). Assessing the present and future probability of Hurricane Harvey's rainfall. *Proceedings of the National Academy of Sciences of the United States of America*, *114*(48), 12681–12684. https://doi.org/10.1073/pnas.1716222114

Enfield, D. B., Mestas-Nuñez, A. M., & Trimble, P. J. (2001). The Atlantic Multidecadal Oscillation and its relation to rainfall and river flows in the continental U.S. *Geophysical Research Letters*, *28*(10), 2077–2080. https://doi.org/10.1029/2000GL012745

Fairchild, I. J., Smith, C. L., Baker, A., Fuller, L., Spötl, C., Mattey, D., et al. (2006). Modification and preservation of environmental signals in speleothems. *Earth-Science Reviews*, *75*(1–4), 105–153. https://doi.org/10.1016/J.EARSCIREV.2005.08.003

Fohlmeister, J., Kromer, B., & Mangini, A. (2011). The influence of soil organic matter age spectrum on the reconstruction of atmospheric ^{14}C levels via stalagmites. *Radiocarbon*, *53*(1), 99–115. https://doi.org/10.1017/S003382220003438X

Fosu, B., He, J., & Liguori, G. (2020). Equatorial Pacific warming attenuated by SST warming patterns in the tropical Atlantic and Indian oceans. *Geophysical Research Letters*, *47*(18), e2020GL088231. https://doi.org/10.1029/2020GL088231

Frappier, A. B., Sahagian, D., Carpenter, S. J., González, L. A., & Frappier, B. R. (2007). Stalagmite stable isotope record of recent tropic cyclone events. *Geology*, *35*(2), 111–114. https://doi.org/10.1130/G23145A.1

Genty, D., Massault, M., Gilmour, M., Baker, A., Verheyden, S., & Kepens, E. (1999). Calculation of past dead carbon proportion and variability by the comparison of AMS ^{14}C and TIMS U/Th ages on two Holocene stalagmites. *Radiocarbon*, *41*(3), 251–270. https://doi.org/10.1017/S003382220005712X

Giannini, A., Chiang, J. C. H., Cane, M. A., Kushnir, Y., & Seager, R. (2001). The ENSO teleconnection to the tropical Atlantic ocean: Contributions of the remote and local SSTs to rainfall variability in the tropical Americas. *Journal of Climate*, *14*(24), 4530–4544. https://doi.org/10.1175/1520-0442(2001)014<4530:TETTTT>2.0.CO;2

Giannini, A., Kushnir, Y., & Cane, M. A. (2000). Interannual variability of Caribbean rainfall, ENSO, and the Atlantic ocean. *Journal of Climate*, *13*(2), 297–311. https://doi.org/10.1175/1520-0442(2000)013<0297:IVOCRE>2.0.CO;2

Gray, S. T., Graumlich, L. J., Betancourt, J. L., & Pederson, G. T. (2004). A tree-ring based reconstruction of the Atlantic Multidecadal Oscillation since 1567 A.D. *Geophysical Research Letters*, *31*(12). https://doi.org/10.1029/2004GL019932

Griffiths, M. L., Fohlmeister, J., Drysdale, R. N., Hua, Q., Johnson, K. R., Hellstrom, J. C., et al. (2012). Hydrological control of the dead carbon fraction in a Holocene tropical speleothem. *Quaternary Geochronology*, *14*, 81–93. https://doi.org/10.1016/j.quageo.2012.04.001

Griffiths, M. L., Johnson, K. R., Pausata, F. S. R., White, J. C., Henderson, G. M., Wood, C. T., et al. (2020). End of Green Sahara amplified mid- to late Holocene megadroughts in mainland Southeast Asia. *Nature Communications*, *11*(1), 4204. https://doi.org/10.1038/s41467-020-17927-6

Gutiérrez-García, G., Beramendi-Orosco, L. E., & Johnson, K. R. (2020). Climate-growth relationships of Pinus pseudostrobus from a tropical mountain cloud forest in northeast Mexico. *Dendrochronologia*, *64*, 125749. https://doi.org/10.1016/j.dendro.2020.125749

He, J., & Soden, B. J. (2017). A re-examination of the projected subtropical precipitation decline. *Nature Climate Change*, *7*(1), 53–57. https://doi.org/10.1038/nclimate3157

Hellstrom, J. (2006). U-Th dating of speleothems with high initial 230 Th using stratigraphical constraint. *Quaternary Geochronology*, *1*, 289–295. https://doi.org/10.1016/j.quageo.2007.01.004

Hendy, C. H. (1971). The isotopic geochemistry of speleothems-I. The calculation of the effects of different modes of formation on the isotopic composition of speleothems and their applicability as palaeoclimatic indicators. *Geochimica et Cosmochimica Acta*, *35*(8), 801–824. https://doi.org/10.1016/0016-7037(71)90127-X

Hidalgo, H. G., Amador, J. A., Alfaro, E. J., & Quesada, B. (2013). Hydrological climate change projections for Central America. *Journal of Hydrology*, *495*, 94–112. https://doi.org/10.1016/j.jhydrol.2013.05.004

Huang, B., Banzon, V. F., Freeman, E., Lawrimore, J., Liu, W., Peterson, T. C., et al. (2015). Extended reconstructed sea surface temperature version 4 (ERSST.v4). Part I: Upgrades and intercomparisons. *Journal of Climate*, *28*(3), 911–930. https://doi.org/10.1175/JCLI-D-14-00006.1.,

Hunter, L. M., Murray, S., & Riosmena, F. (2013). Rainfall patterns and U.S. Migration from rural Mexico. *International Migration Review*, *47*(4), 874–909. https://doi.org/10.1111/imre.12051

Imbol Nkwinkwa, A., Latif, M., & Park, W. (2021). Mean-state dependence of CO_2 -forced tropical Atlantic sector climate change. *Geophysical Research Letters*, *48*(19), e2021GL093803. https://doi.org/10.1029/2021gl093803

Johnson, K. R. (2021). Tales from the underground: Speleothem records of past hydroclimate. *Elements*, *17*(2), 93–100. https://doi.org/10.2138/GSELEMENTS.17.2.93

Kennett, D. J., Breitenbach, S. F. M., Aquino, V. V., Asmerom, Y., Awe, J., Baldini, J. U. L., et al. (2012). Development and disintegration of maya political systems in response to climate change. *Science*, *338*(6108), 788–791. https://doi.org/10.1126/science.1226299

Knutson, T., Camargo, S. J., Chan, J. C. L., Emanuel, K., Ho, C. H., Kossin, J., et al. (2019). Tropical cyclones and climate change assessment. *Bulletin of the American Meteorological Society*, *100*(10), 1987–2007. https://doi.org/10.1175/BAMS-D-18-0189.1

Konecky, B. L., Noone, D. C., & Cobb, K. M. (2019). The influence of competing hydroclimate processes on stable isotope ratios in tropical rainfall. *Geophysical Research Letters*, *46*(3), 1622–1633. https://doi.org/10.1029/2018GL080188

Lachniet, M. S. (2009). Climatic and environmental controls on speleothem oxygen-isotope values. *Quaternary Science Reviews*, *28*(5–6), 412–432. https://doi.org/10.1016/j.quascirev.2008.10.021

Lachniet, M. S., Asmerom, Y., Polyak, V., & Bernal, J. P. (2017). Two millennia of Mesoamerican monsoon variability driven by Pacific and Atlantic synergistic forcing. *Quaternary Science Reviews*, *155*, 100–113. https://doi.org/10.1016/j.quascirev.2016.11.012

Lachniet, M. S., Bernal, J. P., Asmerom, Y., Polyak, V., & Piperno, D. (2012). A 2400 yr Mesoamerican rainfall reconstruction links climate and cultural change. *Geology*, *40*(3), 259–262. https://doi.org/10.1130/G32471.1

Lachniet, M. S., Burns, S. J., Piperno, D. R., Asmerom, Y., Polyak, V. J., Moy, C. M., & Christenson, K. (2004). A 1500-year El Niño/Southern Oscillation and rainfall history for the Isthmus of Panama from speleothem calcite. *Journal of Geophysical Research - D: Atmospheres*, *109*(20), 20117. https://doi.org/10.1029/2004JD004694

Lachniet, M. S., & Patterson, W. P. (2009). Oxygen isotope values of precipitation and surface waters in northern Central America (Belize and Guatemala) are dominated by temperature and amount effects. *Earth and Planetary Science Letters*, *284*(3–4), 435–446. https://doi.org/10.1016/J.EPSL.2009.05.010

Lachniet, M. S., Patterson, W. P., Burns, S., Asmerom, Y., & Polyak, V. (2007). Caribbean and Pacific moisture sources on the Isthmus of Panama revealed from stalagmite and surface water $\delta^{18}O$ gradients. *Geophysical Research Letters*, *34*(1), L01708. https://doi.org/10.1029/2006GL028469

Lases-Hernández, F., Medina-Elizalde, M., & Benoit Frappier, A. (2020). Drip water $\delta^{18}O$ variability in the northeastern Yucatán Peninsula, Mexico: Implications for tropical cyclone detection and rainfall reconstruction from speleothems. *Geochimica et Cosmochimica Acta*, *285*, 237–256. https://doi.org/10.1016/J.GCA.2020.07.008

Li, L., & Chakraborty, P. (2020). Slower decay of landfalling hurricanes in a warming world. *Nature*, *587*(7833), 230–234. https://doi.org/10.1038/s41586-020-2867-7

Magana, V. O., Vázquez, J. L., Párez, J. L., & Pérez, J. B. (2003). Impact of El Niño on precipitation in Mexico. *Geofísica Internacional*, *42*(3), 313–330. Retrieved from http://www.redalyc.org/articulo.oa?id=56842304

Marsh, D. R., Mills, M. J., Kinnison, D. E., Lamarque, J. F., Calvo, N., & Polvani, L. M. (2013). Climate change from 1850 to 2005 simulated in CESM1(WACCM). *Journal of Climate*, *26*(19), 7372–7391. https://doi.org/10.1175/JCLI-D-12-00558.1

Martinez-Lopez, B., Quintanar, A. I., Cabos-Narvaez, W. D., Gay-Garcia, C., & Sein, D. V. (2018). Nonlinear trends and nonstationary oscillations as extracted from annual accumulated precipitation at Mexico city. *Earth and Space Science*, *5*(9), 473–485. https://doi.org/10.1029/2018EA000395

McCabe-Glynn, S., Johnson, K. R., Strong, C., Berkelhammer, M., Sinha, A., Cheng, H., & Edwards, R. L. (2013). Variable North Pacific influence on drought in southwestern North America since AD 854. *Nature Geoscience*, *6*(8), 617–621. https://doi.org/10.1038/ngeo1862

Medina-Elizalde, M., Burns, S. J., Lea, D. W., Asmerom, Y., von Gunten, L., Polyak, V., et al. (2010). High resolution stalagmite climate record from the Yucatán Peninsula spanning the Maya terminal classic period. *Earth and Planetary Science Letters*, *298*(1–2), 255–262. https://doi.org/10.1016/j.epsl.2010.08.016

Méndez, M., & Magaña, V. (2010). Regional aspects of prolonged meteorological droughts over Mexico and central America. *Journal of Climate*, *23*(5), 1175–1188. https://doi.org/10.1175/2009JCLI3080.1

Mestas-Nuñez, A. M., Enfield, D. B., & Zhang, C. (2007). Water vapor fluxes over the Intra-Americas Sea: Seasonal and interannual variability and associations with rainfall. *Journal of Climate*, *20*(9), 1910–1922. https://doi.org/10.1175/JCLI4096.1

Noronha, A. L., Johnson, K. R., Southon, J. R., Hu, C., Ruan, J., & McCabe-Glynn, S. (2015). Radiocarbon evidence for decomposition of aged organic matter in the vadose zone as the main source of speleothem carbon. *Quaternary Science Reviews*, *127*, 37–47. https://doi.org/10.1016/J.QUASCIREV.2015.05.021

Pérez Quezadas, J., Cortés Silva, A., Inguaggiato, S., del Rocío Salas Ortega, M., Cervantes Pérez, J., & Heilweil, V. M. (2015). Meteoric isotopic gradient on the windward side of the Sierra Madre Oriental area, Veracruz - Mexico. *Geofísica Internacional*, *54*(3), 267–276. https://doi.org/10.1016/j.gi.2015.04.021

Rayner, N. A., Parker, D. E., Horton, E. B., Folland, C. K., Alexander, L. V., Rowell, D. P., et al. (2003). Global analyses of sea surface temperature, sea ice, and night marine air temperature since the late nineteenth century. *Journal of Geophysical Research*, *108*(14), 4407. https://doi.org/10.1029/2002jd002670

Reimer, P. J., Bard, E., Bayliss, A., Beck, J. W., Blackwell, P. G., Ramsey, C. B., et al. (2013). Selection and treatment of data for radiocarbon Calibration: An update to the international Calibration (IntCal) Criteria. *Radiocarbon*, *55*(4), 1923–1945. https://doi.org/10.2458/azu_js_rc.55.16955

Risi, C., Bony, S., & Vimeux, F. (2008). Influence of convective processes on the isotopic composition ($\delta^{18}O$ and δD) of precipitation and water vapor in the tropics: 2. Physical interpretation of the amount effect. *Journal of Geophysical Research*, *113*(D19), D19306. https://doi.org/10.1029/2008JD009943

Roy, P. D., Rivero-Navarrete, A., Sánchez-Zavala, J. L., Beramendi-Orosco, L. E., Muthu-Sankar, G., & Lozano-Santacruz, R. (2016). Atlantic Ocean modulated hydroclimate of the subtropical northeastern Mexico since the last glacial maximum and comparison with the southern US. *Earth and Planetary Science Letters*, *434*, 141–150. https://doi.org/10.1016/j.epsl.2015.11.048

Roy, P. D., Vera-Vera, G., Sánchez-Zavala, J. L., Shanahan, T. M., Quiroz-Jiménez, J. D., Curtis, J. H., et al. (2020). Depositional histories of vegetation and rainfall intensity in Sierra Madre Oriental Mountains (northeast Mexico) since the late last glacial. *Global and Planetary Change*, *187*(July 2019), 103136. https://doi.org/10.1016/j.gloplacha.2020.103136

Sachs, J. P., Sachse, D., Smittenberg, R. H., Zhang, Z., Battisti, D. S., & Golubic, S. (2009). Southward movement of the Pacific intertropical convergence zone AD 1400-1850. *Nature Geoscience*, *2*(7), 519–525. https://doi.org/10.1038/ngeo554

Sánchez-Murillo, R., Birkel, C., Welsh, K., Esquivel-Hernández, G., Corrales-Salazar, J., Boll, J., et al. (2016). Key drivers controlling stable isotope variations in daily precipitation of Costa Rica: Caribbean Sea versus Eastern Pacific Ocean moisture sources. *Quaternary Science Reviews*, *131*, 250–261. https://doi.org/10.1016/J.QUASCIREV.2015.08.028

Sánchez-Murillo, R., Esquivel-Hernández, G., Welsh, K., Brooks, E. S., Boll, J., Alfaro-Solís, R., & Valdes-Gonzalez, J. (2013). Spatial and temporal variation of stable isotopes in precipitation across Costa Rica: An analysis of historic GNIP records. *Open Journal of Modern Hydrology*, *3*(4), 226–240. https://doi.org/10.4236/OJMH.2013.34027

Sanders, W. T., Parsons, J. R., & Santley, R. S. (1979). *The Basin of Mexico: Ecological processes in the evolution of a civilization* (p. 561). Academic Press.

Schlesinger, M. E., & Ramankutty, N. (1994). An oscillation in the global climate system of period 65-70 years. *Nature*, *367*(6465), 723–726. https://doi.org/10.1038/367723a0

Schneider, U., Becker, A., Finger, P., Meyer-Christoffer, A., Rudolf, B., & Ziese, M. (2011). *GPCC full data Reanalysis version 6.0 at 0.5: Monthly land-surface precipitation from rain-gauges built on GTS-based and historic data*. https://doi.org/10.5676/DWD_GPCC/FD_M_V7_050

Seager, R., & Hoerling, M. (2014). Atmosphere and ocean origins of North American droughts. *Journal of Climate*, *27*(12), 4581–4606. https://doi.org/10.1175/JCLI-D-13-00329.1

Smith, K. L., Neely, R. R., Marsh, D. R., & Polvani, L. M. (2015). The specified chemistry Whole atmosphere Community climate model (SC-WACCM). *Journal of Advances in Modeling Earth Systems*, *6*(3), 883–901. https://doi.org/10.1002/2014MS000346

St. George, S., Meko, D. M., & Cook, E. R. (2010). The seasonality of precipitation signals embedded within the North American Drought Atlas. *The Holocene*, *20*(6), 983–988. https://doi.org/10.1177/0959683610365937

Stahle, D. W., Cook, E. R., Burnette, D. J., Torbenson, M. C. A., Howard, I. M., Griffin, D., et al. (2020). Dynamics, variability, and change in seasonal precipitation reconstructions for North America. *Journal of Climate*, *33*(8), 3173–3195. https://doi.org/10.1175/JCLI-D-19-0270.1

Stahle, D. W., Cook, E. R., Burnette, D. J., Villanueva, J., Cerano, J., Burns, J. N., et al. (2016). The Mexican Drought Atlas: Tree-ring reconstructions of the soil moisture balance during the late pre-Hispanic, colonial, and modern eras. *Quaternary Science Reviews*, *149*, 34–60. Pergamon. https://doi.org/10.1016/j.quascirev.2016.06.018

Ting, M., Kushnir, Y., Seager, R., & Li, C. (2009). Forced and internal twentieth-century SST trends in the North Atlantic. *Journal of Climate*, *22*(6), 1469–1481. https://doi.org/10.1175/2008JCLI2561.1

Villanueva-Diaz, J., Stahle, D. W., Luckman, B. H., Cerano-Paredes, J., Therrell, M. D., Cleaveland, M. K., & Cornejo-Oviedo, E. (2007). Winter-spring precipitation reconstructions from tree rings for northeast Mexico. *Climatic Change*, *83*(1–2), 117–131. https://doi.org/10.1007/s10584-006-9144-0

Vuille, M., & Werner, M. (2005). Stable isotopes in precipitation recording South American summer monsoon and ENSO variability: Observations and model results. *Climate Dynamics*, *25*(4), 401–413. https://doi.org/10.1007/s00382-005-0049-9

Wang, C. (2007). Variability of the Caribbean low-level jet and its relations to climate. *Climate Dynamics*, *29*(4), 411–422. https://doi.org/10.1007/s00382-007-0243-z

Wang, C., & Lee, S. K. (2007). Atlantic warm pool, Caribbean low-level jet, and their potential impact on Atlantic hurricanes. *Geophysical Research Letters*, *34*(2), L02703. https://doi.org/10.1029/2006GL028579

Wise, E. K., & Dannenberg, M. P. (2019). Climate factors leading to Asymmetric extreme capture in the tree-ring record. *Geophysical Research Letters*, *46*(6), 3408–3416. https://doi.org/10.1029/2019GL082295

Wogau, K. H., Arz, H. W., Böhnel, H. N., Nowaczyk, N. R., & Jungjae, P. (2019). High resolution paleoclimate and paleoenvironmental reconstruction in the Northern Mesoamerican Frontier for Prehistory to Historical times. *Quaternary Science Reviews*, *226*, 106001. https://doi.org/10.1016/j.quascirev.2019.106001

Wright, K., Johnson, K., Marks, G. S., Mcgee, D., Goldsmith, G. R., Tabor, C., et al. (2021). *Thermodynamics Control Precipitation in NE Mexico on Orbital to Millennial Timescales* (Vol. 25). https://doi.org/10.21203/RS.3.RS-611282/V1

Yoshimura, K., Kanamitsu, M., Noone, D., & Oki, T. (2008). Historical isotope simulation using reanalysis atmospheric data. *Journal of Geophysical Research*, *113*(19), D19108. https://doi.org/10.1029/2008JD010074

References From the Supporting Information

Black, D. E., Abahazi, M. A., Thunell, R. C., Kaplan, A., Tappa, E. J., & Peterson, L. C. (2007). An 8-century tropical Atlantic SST record from the Cariaco Basin: Baseline variability, twentieth-century warming, and Atlantic hurricane frequency. *Paleoceanography*, *22*(4), PA4204. https://doi.org/10.1029/2007PA001427

Borsato, A., Johnston, V. E., Frisia, S., Miorandi, R., & Corradini, F. (2016). Temperature and altitudinal influence on karst dripwater chemistry: Implications for regional-scale palaeoclimate reconstructions from speleothems. *Geochimica et Cosmochimica Acta*, *177*, 275–297. https://doi.org/10.1016/j.gca.2015.11.043

Fensterer, C., Scholz, D., Hoffmann, D. L., Spötl, C., Schröder-Ritzrau, A., Horn, C., et al. (2013). Millennial-scale climate variability during the last 12.5 ka recorded in a Caribbean speleothem. *Earth and Planetary Science Letters*, *361*, 143–151. https://doi.org/10.1016/j.epsl.2012.11.019

Ford, D. C. (2000). *Deep phreatic caves and groundwater systems of the Sierra de El Abra, Mexico. Speleogenesis: Evolution of Karst aquifers: Huntsville, Alabama*. National Speleological. 325–331.

Gary, M. S. J. (2006). *Volcanogenic Karstification of Sistema Zacatón* (pp. 79–89). https://doi.org/10.1130/2006.2404(08)

Gram, W. K., & Faaborg, J. (1997). The distribution of neotropical migrant birds wintering in the El Cielo biosphere reserve, Tamaulipas, Mexico. *The Condor: Ornithological Applications*, *99*(3), 658–670. https://doi.org/10.2307/1370478

Hammer, Ø., Harper, D. A. T., & Ryan, P. D. (2001). Past: Paleontological statistics software package for education and data analysis. *Palaeontologia Electronica*, *4*(1), 178. Retrieved from http://palaeo-electronica.orghttp//palaeo-electronica.org/2001_1/past/issue1_01.htm

Johnson, K. R., Hu, C., Belshaw, N. S., & Henderson, G. M. (2006). Seasonal trace-element and stable-isotope variations in a Chinese speleothem: The potential for high-resolution paleomonsoon reconstruction. *Earth and Planetary Science Letters*, *244*(1–2), 394–407. https://doi.org/10.1016/j.epsl.2006.01.064

Kovaltsov, G. A., Mishev, A., & Usoskin, I. G. (2012). A new model of cosmogenic production of radiocarbon ^{14}C in the atmosphere. *Earth and Planetary Science Letters*, *337*(338), 114–120. https://doi.org/10.1016/j.epsl.2012.05.036

Martín-Chivelet, J., Belén Muñoz-García, M., Cruz, J. A., Ortega, A. I., Turrero, M. J., & Jones, B. (2017). *Speleothem Architectural Analysis: Integrated approach for stalagmite-based paleoclimate research*. https://doi.org/10.1016/j.sedgeo.2017.03.003

Schimmelmann, A., Hendy, I. L., Dunn, L., Pak, D. K., & Lange, C. B. (2013). Revised ~2000-year chronostratigraphy of partially varved marine sediment in Santa Barbara Basin, California. *GFF*, *135*(3–4), 258–264. https://doi.org/10.1080/11035897.2013.773066

Schulz, M., & Mudelsee, M. (2002). REDFIT: Estimating red-noise spectra directly from unevenly spaced paleoclimatic time series. *Computers & Geosciences*, *28*(3), 421–426. https://doi.org/10.1016/S0098-3004(01)00044-9

Tierney, J. E., Abram, N. J., Anchukaitis, K. J., Evans, M. N., Giry, C., Kilbourne, K. H., et al. (2015). Tropical sea surface temperatures for the past four centuries reconstructed from coral archives. *Paleoceanography*, *30*(3), 226–252. https://doi.org/10.1002/2014PA002717

Winter, A., Miller, T., Kushnir, Y., Sinha, A., Timmermann, A., Jury, M. R., et al. (2011). Evidence for 800 years of North Atlantic multi-decadal variability from a Puerto Rican speleothem. *Earth and Planetary Science Letters*, *308*(1–2), 23–28. https://doi.org/10.1016/j.epsl.2011.05.028

Winter, A., Zanchettin, D., Lachniet, M., Vieten, R., Pausata, F. S. R., Ljungqvist, F. C., et al. (2020). Initiation of a stable convective hydroclimatic regime in Central America circa 9000 years BP. *Nature Communications*, *11*(1), 1–8. https://doi.org/10.1038/s41467-020-14490-y